

LinearFold: linear-time approximate RNA folding by 5'-to-3' dynamic programming and beam search

Liang Huang^{1,2,*}, He Zhang^{2,†}, Dezhong Deng^{1,†}, Kai Zhao^{1,‡}, Kaibo Liu^{1,2}, David A. Hendrix^{3,1} and David H. Mathews^{4,5,6}

¹School of Electrical Engineering and Computer Science, Oregon State University, Corvallis, OR 97330, USA, ²Baidu Research USA, Sunnyvale, CA 94089, USA, ³Department of Biochemistry & Biophysics, Oregon State University, and ⁴Department of Biochemistry & Biophysics, ⁵Center for RNA Biology, and ⁶Department of Biostatistics & Computational Biology, University of Rochester Medical Center, Rochester, NY 48306, USA

*To whom correspondence should be addressed.

†The authors wish it to be known that these authors contributed equally (co-second authors).

‡: Present address: Google, Inc, New York, NY 10011, USA.

Abstract

Motivation: Predicting the secondary structure of an RNA sequence is useful in many applications. Existing algorithms (based on dynamic programming) suffer from a major limitation: their runtimes scale *cubically* with the RNA length, and this slowness limits their use in genome-wide applications.

Results: We present a novel alternative $O(n^3)$ -time dynamic programming algorithm for RNA folding that is amenable to heuristics that make it run in $O(n)$ time and $O(n)$ space, while producing a high-quality approximation to the optimal solution. Inspired by incremental parsing for context-free grammars in computational linguistics, our alternative dynamic programming algorithm scans the sequence in a left-to-right (5'-to-3') direction rather than in a bottom-up fashion, which allows us to employ the effective beam pruning heuristic. Our work, though inexact, is the first RNA folding algorithm to achieve linear runtime (and linear space) without imposing constraints on the output structure. Surprisingly, our approximate search results in even higher overall accuracy on a diverse database of sequences with known structures. More interestingly, it leads to significantly more accurate predictions on the longest sequence families in that database (16S and 23S Ribosomal RNAs), as well as improved accuracies for long-range base pairs (500+ nucleotides apart), both of which are well known to be challenging for the current models.

Availability: Our source code is available at <https://github.com/LinearFold/LinearFold>, and our webserver is at <http://linearfold.org> (sequence limit: 100,000nt).

Contact: liang.huang.sh@gmail.com

Supplementary information: [Supplementary data](#) are available at *Bioinformatics* online (attached [here](#)).

1 Introduction

Ribonucleic acid (RNA) is involved in numerous cellular processes (Eddy, 2001). The dual nature of RNA as both a genetic material and functional molecule led to the RNA World hypothesis, that RNA was the first molecule of life (Gilbert, 1986), and this dual nature has also been utilized to develop *in vitro* methods to evolve functional sequences (Joyce, 1994). Furthermore, RNA is an important drug target and agent (Angelbello *et al.*, 2018; Sazani *et al.*, 2002; Crooke, 2004; Childs-Disney *et al.*, 2007; Gareiss *et al.*, 2008; Castanotto and Rossi, 2009; Palde *et al.*, 2010).

Predicting the secondary structure of an RNA sequence, defined as the set of all canonical base pairs (A–U, G–C, G–U, see Fig. 1A), is an important and challenging problem (Seetin and Mathews, 2012; Hofacker and Lorenz, 2014). Knowing the structure reveals crucial information

about the RNA's function, which is useful in many applications ranging from ncRNA detection (Gruber *et al.*, 2010; Washietl *et al.*, 2012; Fu *et al.*, 2015) to the design of oligonucleotides for knockdown of message (Lu and Mathews, 2008; Tafer *et al.*, 2008). Since experimentally determining the structure is expensive and time consuming, and given the overwhelming increase in genomic data (about 10^{21} base-pairs per year) (Stephens *et al.*, 2015), computational methods have been widely used as an alternative to automatically predict the structure. Widely used systems such as RNAstructure (Mathews and Turner, 2006), Vienna RNAfold (Lorenz *et al.*, 2011), CONTRAfold (Do *et al.*, 2006) and CentroidFold (Sato *et al.*, 2009), all use virtually the same dynamic programming (DP) algorithm (Nussinov *et al.*, 1978; Zuker and Stiegler, 1981) to find the best-scoring (lowest free energy, maximum expected accuracy, or best model score) structure (Mathews and Turner, 2006; Washietl *et al.*, 2012). However, this set of algorithms, borrowed from computational linguistics (Kasami,

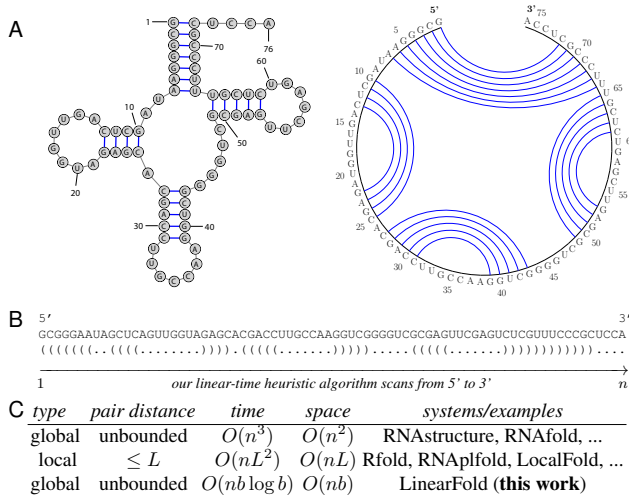


Fig. 1. Summary of our work. **A:** secondary structure representations of *E. coli* tRNA^{Gly}; **B:** the corresponding dot-bracket format and an illustration of our algorithm, which scans the sequence left-to-right, and tags each nucleotide as “.” (unpaired), “(” (to be paired with a future nucleotide) or “)” (paired with a previous nucleotide). **C:** comparison between our work and existing ones. L is the limit of pair distance in local folding methods (often ≤ 150), and b is the beam size in our work (default 100). Our algorithm, though approximate, is the first to achieve linear runtime without imposing constraints on the output structure.

1965; Younger, 1967), has a running time of $O(n^3)$ that scales cubically with the sequence length n , which is too slow for long RNA sequences (Lange et al., 2012).

As an alternative, faster algorithms that predict only a restricted subset of structures have been proposed. On the one hand, local folding methods such as Rfold (Kiryu et al., 2008), Vienna RNAplfold (Bernhart et al., 2006), and LocalFold (Lange et al., 2012) run in linear time but only predict base pairs up to L nucleotides apart ($L \leq 150$ in the literature; see Fig. 1C). On the other hand, due to the prohibitive cubic runtime of standard methods, it has been a common practice to divide long RNA sequences into short segments (e.g., $\leq 700nt$) and predict structures within each segment only (Watts et al., 2009; Andronescu et al., 2007; Licon et al., 2010). All these local methods omit long-range base pairs, which theoretical and experimental studies have demonstrated to be common in natural RNAs, especially between the 5' and 3' ends (Seetin and Mathews, 2012; Lai et al., 2018; Li and Reidys, 2018).

We instead design **LinearFold**, an approximate algorithm that is the first in RNA folding to achieve linear runtime (and linear space) without imposing constraints on the output structure such as base pair distance. While the classical $O(n^3)$ -time algorithm is bottom-up, making it hard to linearize, ours runs left-to-right (i.e., 5' to-3'), incrementally tagging each nucleotide in the dot-bracket format (Fig. 1B). While this naive version runs in the exponential time of $O(3^n)$, we borrow an efficient packing idea from computational linguistic (Tomita, 1988) that reduces the runtime back to $O(n^3)$. This novel left-to-right $O(n^3)$ dynamic program is also a contribution of this paper. Furthermore, on top of this exact algorithm, we apply beam search, a popular heuristic to prune the search space (Huang and Sagae, 2010), which keeps only the top b highest-scoring (or lowest energy) states for each prefix of the input sequence, resulting in an $O(nb \log b)$ time approximate search algorithm, where b is the beam size chosen by the user.

Our approach can “linearize” any dynamic programming-based pseudoknot-free RNA folding system. In particular, we demonstrate two

versions of LinearFold, LinearFold-V using the thermodynamic free energy model (Mathews et al., 2004) from Vienna RNAfold (Lorenz et al., 2011), and LinearFold-C using the machine learned model from CONTRAfold (Do et al., 2006). We evaluate our systems on a diverse dataset of RNA sequences with well-established structures, and show that while being substantially more efficient, LinearFold leads to even higher average accuracies over all families, and more interestingly, LinearFold is significantly more accurate than the exact search methods on the longest families, 16S and 23S Ribosomal RNAs. In addition, LinearFold is also more accurate on long-range base pairs, which is well known to be a challenging problem for the current models (Amman et al., 2013).

Finally, our work establishes a new connection among computational linguistics, compiler theory, and RNA folding (see Supplementary Fig. S17).

2 The LinearFold Algorithm

2.1 Problem Formulation

Given an RNA sequence $\mathbf{x} = x_1x_2 \dots x_n$, where each $x_i \in \{A, C, G, U\}$, the secondary structure prediction problem aims to find the best-scoring pseudoknot-free structure $\hat{\mathbf{y}}$ by maximizing a scoring function $sc_{\mathbf{w}}$ (e.g., model score or negative free energy) where \mathbf{w} are the model parameters:

$$\hat{\mathbf{y}} = \underset{\mathbf{y} \in \mathcal{Y}(\mathbf{x})}{\operatorname{argmax}} sc_{\mathbf{w}}(\mathbf{x}, \mathbf{y}). \quad (1)$$

Here $\mathcal{Y}(\mathbf{x})$ is the set of all possible pseudoknot-free secondary structures for input \mathbf{x} of length n

$$\{\mathbf{y} \in \{., (,)\}^n \mid \text{balanced}(\mathbf{y}), \text{valid}(\mathbf{x}, \text{pairs}(\mathbf{y}))\}$$

where $\text{balanced}(\mathbf{y})$ checks if \mathbf{y} has balanced brackets, $\text{valid}(\mathbf{x}, \text{pairs}(\mathbf{y}))$ checks if all pairs in \mathbf{y} are valid (CG, AU, GU), and $\text{pairs}(\mathbf{y})$ returns the set of (i, j) pairs where x_i and x_j form a base pair in \mathbf{y} , e.g., $\text{pairs}(((.))) = \{(1, 5), (2, 4)\}$. See Supplementary Section A for detailed definitions.

All dynamic programming-based prediction algorithms, including ours, require the scoring function $sc_{\mathbf{w}}(\mathbf{x}, \cdot)$ to decompose to smaller structures. For simplicity of presentation, in the main text we will use a very simple decomposition to individual pairs and unpaired nucleotides:

$$sc_{\mathbf{w}}(\mathbf{x}, \mathbf{y}) = \sum_{(i,j) \in \text{pairs}(\mathbf{y})} w_{x_i x_j} + \sum_{i \in \text{unpaired}(\mathbf{y})} w_{\text{unpaired}} \quad (2)$$

In this framework we can assign different scores for different pairs, and incur a penalty for each unpaired nucleotide. For the example in Fig. 2, we simply set $w_{CG} = w_{AU} = w_{GU} = 1$ and $w_{\text{unpaired}} = -0.1$; therefore, $sc_{\mathbf{w}}(\text{“CCAGG”}, \text{“((.))”}) = 2w_{CG} + w_{\text{unpaired}} = 1.9$.

In reality, however, the actual scoring functions used by CONTRAfold, RNAfold, and our LinearFold are much more complex, and they decompose into individual loops. See Supplementary Section B for details.

2.2 Idea 0: Brute-Force Search: $O(3^n)$

The initial idea, introduced in Fig. 1B, is to scan the RNA sequence left-to-right, maintaining a *stack* along the way, and performing one of the three actions (push, skip, or pop) at each step. More formally, we denote each *state* at step j ($j = 0 \dots n$) as a tuple along with a score s :

$$\langle \mathbf{y}, \sigma, j \rangle: s,$$

where \mathbf{y} is the (sub)structure for the prefix $x_1 \dots x_j$, and σ is the stack consisting of unmatched opening bracket positions in \mathbf{y} . For example, in

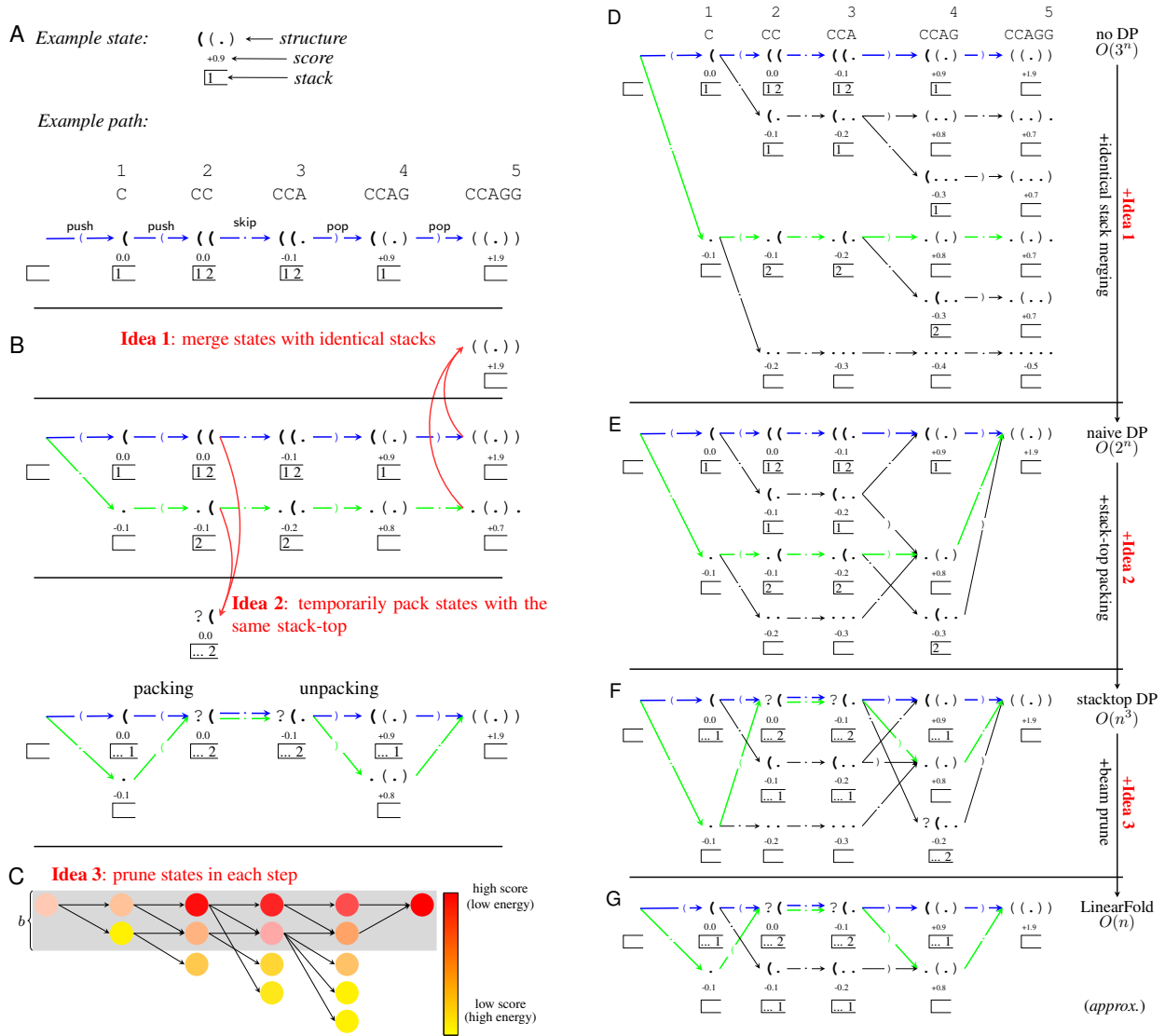


Fig. 2. Illustration of the LinearFold approach, using a short sequence CCAGG and the simple scoring function (Eq. 2). **A:** an example state and an example (actually optimal) path, showing states (predicted prefix structures), actions (push “(”, skip “.”, and pop “)”), and stacks (unpaired open brackets which are shown in bold in states). **B:** two example paths (the optimal one in blue and a suboptimal one in green) and two essential ideas of left-to-right dynamic programming: merging equivalent states with identical stacks (Idea 1) and packing temporarily equivalent states sharing the same stack top, and corresponding unpacking upon pop (Idea 2). **C:** illustration of beam search, which keeps top b states (those in the shaded region) per step (Idea 3). **D:** the whole search space of the naive algorithm ($O(3^n)$ time). **E:** improving to $O(2^n)$ time with Idea 1. **F:** further improving to $O(n^3)$ time with Idea 2. **G:** further improving to $O(n)$ time (but with approximate search) with Idea 3. In **B, F,** and **G,** each green/blue arrow pair $? \rightarrow ?$ is actually a single arrow, denoting two paths temporarily packed as one; we draw paired arrows to highlight that two states $(.$ and $(($ are performing skip action together. Note the version up to Idea 2 is exact and worst-case $O(n^3)$ time.

step 4, if $y = “(.)”$, then $\sigma = [1]$ and $s = 0.9$ (see Fig. 2A); note that we denote open brackets in bold. Each state at step j can transition into a subsequent state of step $j+1$, taking one of the three actions:

1. push: label x_{j+1} as “(” for it to be paired with a downstream nucleotide, and pushing $j+1$ on to the stack, notated:

$$\frac{\langle \mathbf{y}, \sigma, j \rangle : s}{\langle \mathbf{y} \circ ‘(’, \sigma[(j+1), j+1] \rangle : s}$$

2. skip: label x_{j+1} as “.” (unpaired and skipped):

$$\frac{\langle \mathbf{y}, \sigma, j \rangle : s}{\langle \mathbf{y} \circ ‘.’, \sigma, j+1 \rangle : s + w_{\text{unpaired}}}$$

3. pop: label x_{j+1} as “)” paired with the upstream nucleotide x_i where i is the top of the stack, and pop i (if $x_i x_{j+1}$ pair is allowed):

$$\frac{\langle \mathbf{y}, \sigma[i, j] \rangle : s}{\langle \mathbf{y} \circ ‘)’, \sigma, j+1 \rangle : s + w_{x_i x_{j+1}}}$$

We start with the init state $\langle ‘(’, [], 0 \rangle : 0$ and finish with any state $\langle \mathbf{y}, [], n \rangle : s$ with an empty stack (ensuring the output is a well-balanced dot-bracket sequence). See Fig. 2A for an example path for input sequence CCAGG, and Fig. 2D for all valid paths.

The above procedure describes a naive exhaustive search without dynamic programming which has exponential runtime $O(3^n)$, as there are up to three actions per step (see Fig. 2D).

Next, Fig. 2B sketches the two key dynamic programming ideas that speed up this algorithm to $O(n^3)$ by merging and packing states.

2.3 Idea 1 (DP): Merge States with Identical Stacks: $O(2^n)$

We first observe that different states can have the same stack; for example, in step 5, both “. (.) .” and “. (.) .” have the same empty stack (see Fig. 2B, Idea 1); and in step 4, both “. . .” and “. (.) .” have the same stack [1] (see Fig. 2D). These states can be merged, because even though they have different histories, going forward they are exactly equivalent. After merging we save the state with the highest score and discard all others which have no potential to lead to the optimal structure. More formally, we merge two states with the same stack:

$$\left. \begin{array}{l} \langle \mathbf{y}, \sigma, j \rangle : s \\ \langle \mathbf{y}', \sigma, j \rangle : s' \end{array} \right\} \rightarrow \langle \sigma, j \rangle : \langle \mathbf{y}'', s'' \rangle$$

where

$$\langle \mathbf{y}'', s'' \rangle = \begin{cases} \langle \mathbf{y}, s \rangle & \text{if } s > s' \\ \langle \mathbf{y}', s' \rangle & \text{otherwise} \end{cases}$$

This algorithm is faster but still has exponential $O(2^n)$ time as there are exponentially many different stacks (see Fig. 2E).

2.4 Idea 2 (DP): Pack Temporarily Equivalent States: $O(n^3)$

We further observe that even though some states have different stacks, they might share the same stack top. For example, in step 2, “. (” and “. (” have [2] and [1,2] as their stacks, resp., but with the same stack top 2. Our key insight is that two states with the same stack-top are “temporarily equivalent” and can be “packed” as they would behave equivalently until the stack-top open bracket is closed (i.e., matched), after which they “unpack” and diverge. As shown in Fig. 2B (Idea 2), both “. (” and “. (” are looking for a “G” to match with the stack top $x_2 = \text{“C”}$, and can be packed as “. (” with stack [..2] where “?” and “...” represent histories that are not important for now. After skipping the next nucleotide $x_3 = \text{“A”}$, they become “. (.” and upon matching the next nucleotide $x_4 = \text{“G”}$ with the stack-top $x_2 = \text{“C”}$, they unpack, resulting in “. (.)” and “. (.)”.

More formally, two states $\langle \sigma | i, i \rangle : \langle \mathbf{y}, s \rangle$ and $\langle \sigma' | i, i \rangle : \langle \mathbf{y}', s' \rangle$ sharing the same stack top can be packed:

$$\left. \begin{array}{l} \langle \sigma | i, i \rangle : \langle \mathbf{y}, s \rangle \\ \langle \sigma' | i, i \rangle : \langle \mathbf{y}', s' \rangle \end{array} \right\} \rightarrow \langle i, i \rangle : \langle (, 0) \rangle$$

Note that (a) we only need two indices to index the packed state; (b) we omit the ?’s since they contain no information; and (c) somewhat counterintuitively, the resulting packed state’s (sub)structure and score, $\langle (, 0) \rangle$ do not depend on the original states before packing. More formally, for any packed state $\langle i, j \rangle : \langle \mathbf{y}, s \rangle$, its \mathbf{y} is a substructure only for the substring $x_i \dots x_j$, and its score s is also for that portion only, i.e., $s = sc_{\mathbf{w}}(x_i \dots x_j, \mathbf{y})$. We can grow it by skip

$$\frac{\langle i, j \rangle : \langle \mathbf{y}, s \rangle}{\langle i, j+1 \rangle : \langle \mathbf{y} \circ \cdot, s + w_{\text{unpaired}} \rangle}$$

or push actions

$$\frac{\langle i, j \rangle : \langle \mathbf{y}, s \rangle}{\langle j+1, j+1 \rangle : \langle (, 0) \rangle}$$

The pop action is more involved. If x_i and x_{j+1} match, we pop i , but where can we find the “previous stack top”? It is *not* specified in the

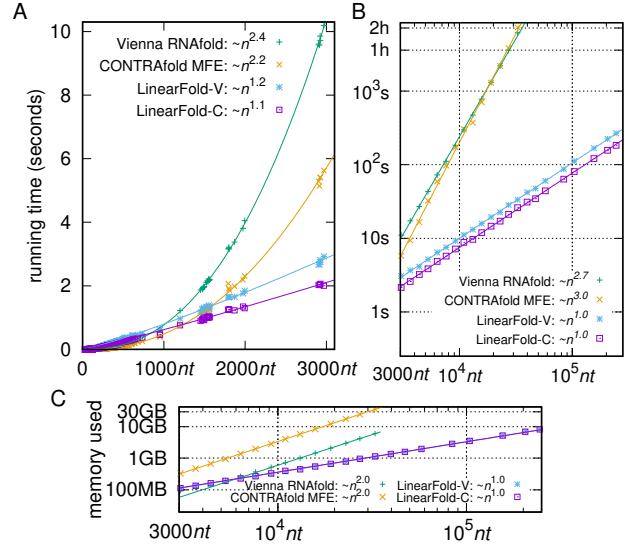


Fig. 3. Efficiency and scalability of LinearFold. **A:** runtime comparisons on the ArchiveII dataset with the two baselines, CONTRAfold MFE and Vienna RNAfold. **B:** runtime comparisons on the RNACentral dataset (log-log). **C:** memory usage comparisons (RNACentral set, log-log). LinearFold uses $O(n)$ time and memory, being substantially faster and slimmer than the $O(n^3)$ -time, $O(n^2)$ -space, baselines on long sequences.

packed state. Therefore, we need to find a state $\langle k, i-1 \rangle : \langle \mathbf{y}', s' \rangle$ that combines with the current state:

$$\frac{\langle k, i-1 \rangle : \langle \mathbf{y}', s' \rangle \quad \langle i, j \rangle : \langle \mathbf{y}, s \rangle}{\langle k, j+1 \rangle : \langle \mathbf{y}' \circ \mathbf{y} \circ \cdot, s' + s + w_{x_i x_{j+1}} \rangle}$$

This version (see Fig. 2F) runs in worst-case $O(n^3)$ time, because the pop step involve three free indices. It guarantees to return the optimal-scoring structure. It is inspired by a well-established algorithm in natural language parsing (Tomita, 1988; Huang and Sagae, 2010); see Supplementary Fig. S17. Although this $O(n^3)$ runtime is the same as those classical bottom-up ones, its unique left-to-right nature makes it amenable to $O(n)$ beam search.

2.5 Idea 3 (Approximate Search): Beam Pruning: $O(n)$

We further employ beam pruning (Huang et al., 2012), a popular heuristic widely used in computational linguistics, to reduce the complexity from $O(n^3)$ to $O(n)$, but with the cost of exact search. Basically, at each step j , we only keep the b top-scoring (lowest-energy) states and prune the other, less promising, ones (because they are less likely to be part of the optimal final structure). This results in an approximate search algorithm in $O(nb^2)$ time, depicted in Figure 2C and G. On top of beam search, we borrow k -best parsing (Huang and Chiang, 2005) to reduce the runtime to $O(nb \log b)$. Here the beam size b is a small constant (by default 100) so the overall runtime is linear in n . We will show that our approximate search achieves even higher overall accuracy than the classical exact search methods. The space complexity is $O(nb)$. See Supplementary Fig. S16 for the real system. There are two minor restrictions in our real system: the length of an interior loop is bounded by $30nt$ (a standard limit found in most existing RNA folding software such as CONTRAfold), so is the leftmost ($5'$ -end) unpaired segment of a multiloop (new constraint). These conditions are valid for 37°C , and no violations were found in the ArchiveII dataset.

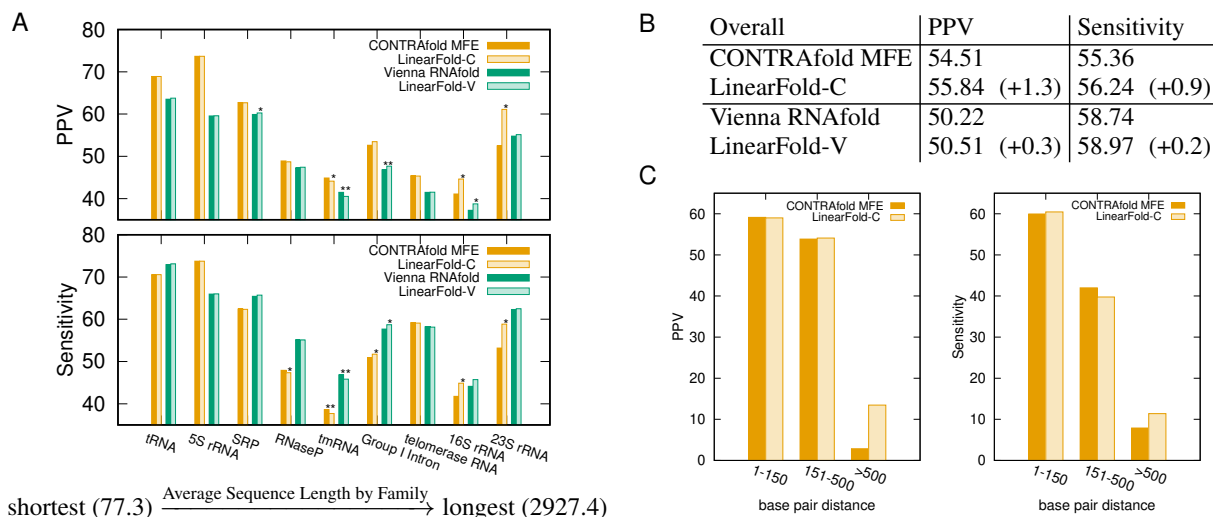


Fig. 4. Accuracy of LinearFold. **A:** Each bar represents PPV/sensitivity averaged over all sequences in one family. Statistical significance is marked as $*$ ($0.01 \leq p < 0.05$) or $**$ ($p < 0.01$). See Table S11 for details. **B:** The overall accuracies, averaging over all families. **C:** Each bar represents the overall PPV/sensitivity of all base pairs in a certain length range across all sequences. Supplementary Fig. S11 shows a similar result for LinearFold-V. Overall, LinearFold outperforms exact search baselines, esp. on longer families and long-range pairs.

3 Results

3.1 Efficiency and Scalability

We compare LinearFold’s efficiency with classical cubic-time algorithms represented by CONTRAFold (Version 2.02) and Vienna RNAfold (Version 2.4.10) (<http://contra.stanford.edu/> and https://www.tbi.univie.ac.at/RNA/download/sourcecode/2_4_x/ViennaRNA-2.4.10.tar.gz). We use two datasets: (a) the ArchiveII dataset (Sloma and Mathews, 2016), a diverse set of RNA sequences with known structures (<http://rna.urmc.rochester.edu/pub/archiveII.tar.gz>); we removed those sequences found in the S-Processed set. See Supplementary Table S11 for details, and (b) a sampled subset of RNACentral (The RNACentral Consortium, 2017) (<https://rnacentral.org/>), a comprehensive set of ncRNA sequences from many databases. While ArchiveII contains sequences of 3,000nt or less, RNACentral has many much longer ones, with the longest being 244,296nt (Homo Sapiens Transcript NONHSAT168677.1, from the NONCODE database (Zhao *et al.*, 2016)). We run all programs (compiled by GCC 4.9.0) on Linux, with 3.40GHz Intel Xeon E3-1231 CPU and 32G memory.

Figure 3A shows that on the relatively short ArchiveII set, LinearFold’s runtime scales almost linearly with the sequence length, while the two baselines have superquadratic runtimes. On the much longer RNACentral set, Figure 3B shows strictly linear runtime for LinearFold and near-cubic runtimes for the baselines, which agrees with the asymptotic analyses and suggests that the minor deviations from the theoretical runtimes are due to the short sequence lengths in the ArchiveII set. For a sequence of $\sim 10,000$ nt (e.g., the HIV genome), LinearFold takes only 8 seconds while the baselines take 4 minutes. For a sequence of 32,753nt, LinearFold takes 26 seconds while CONTRAFold and RNAfold take 2 and 1.7 hours, resp.

In addition, LinearFold uses only $O(n)$ memory (Fig. 3C). The classical $O(n^3)$ -time algorithm uses $O(n^2)$ space, because it needs to solve the best-scoring substructure for each substring $[i, j]$ bottom-up. LinearFold, by contrast, uses $O(n)$ space thanks to left-to-right beam search, and is the first $O(n)$ -space algorithm to be able to predict base pairs of unbounded distance. It is able to fold the longest sequence in RNACentral (244,296nt) within 3 minutes while neither CONTRAFold

or RNAfold runs on anything longer than 32,767nt due to datastructure limitations. As a result, the sequence limit on our web server (10^5 nt, see abstract) is 10x that of RNAfold web server (the previous largest), being by far the largest limit among all available servers (as of March 2019). The curve-fittings in Fig. 3 were done log-log in gnuplot with $n > 10^3$ in A, $n > 3 \times 10^3$ in B, and $n > 10^4$ in C, to focus on the asymptotics.

3.2 Accuracy

We next compare LinearFold with the two baselines in accuracy, reporting both Positive Predictive Value (PPV, the fraction of predicted pairs in the known structure) and sensitivity (the fraction of known pairs predicted) on each RNA family in the ArchiveII dataset, allowing correctly predicted pairs to be offset by one nucleotide as compared to the known structure (Sloma and Mathews, 2016); we also report exact match accuracies in Supplementary Table S12. We test statistical significance using a paired, one-sided permutation test, following (Aghaeepour and Hoos, 2013).

Figure 4 shows that LinearFold is more accurate than the baselines, and interestingly, this advantage is more pronounced on longer sequences. Individually, LinearFold-C (the LinearFold implementation of the CONTRAFold model) is significantly more accurate in sensitivity than CONTRAFold on one family (Group I Intron), and both PPV/sensitivity on two families (16S and 23S ribosomal RNAs), with the last two being the longest families in this dataset, where they have average lengths 1548nt and 2927nt, and enjoyed +3.56%/+3.09% and +8.65%/+5.66% (absolute) improvements in PPV/sensitivity, respectively. LinearFold-V (the LinearFold implementation of the Vienna RNAfold model) also outperforms RNAfold with significant improvements in PPV on two families (SRP and 16S rRNA), and both PPV/sensitivity on one family (Group I Intron). Overall (across all families), LinearFold-C outperforms CONTRAFold by +1.3%/+0.9% PPV/sensitivity, while LinearFold-V outperforms RNAfold by +0.3%/+0.2%. See Supplementary Table S11 for details.

Long-range base pairs are notoriously difficult to predict under current models (Amman *et al.*, 2013). Interestingly, LinearFold is more accurate in both PPV and sensitivity than the exact search algorithm for long-range base pairs of nucleotides greater than 500 nucleotides apart, as

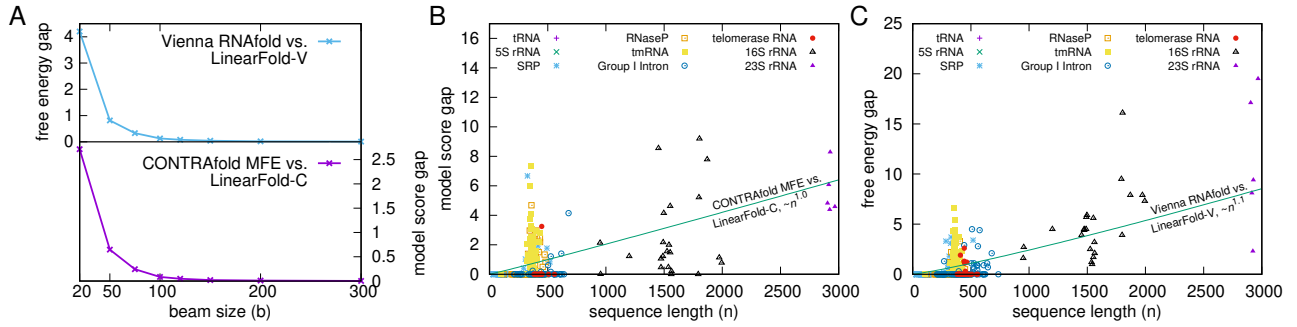


Fig. 5. Search error (model score gap or free energy gap $\Delta\Delta G$). **A:** average free energy gap (Vienna RNAfold vs. LinearFold-V) and model cost gap (CONTRAFold MFE vs. LinearFold-C) with varying beam size; the search error shrinks with beam size, quickly converging to 0. **B and C:** the search error (or gap) grows linearly with sequence length. Here tmRNA is the outlier with disproportionately severe search errors, which can explain the slightly worse accuracies of LinearFold on tmRNA in Fig. 4A. See Supplementary Fig. S13 for a close-up on short sequences.

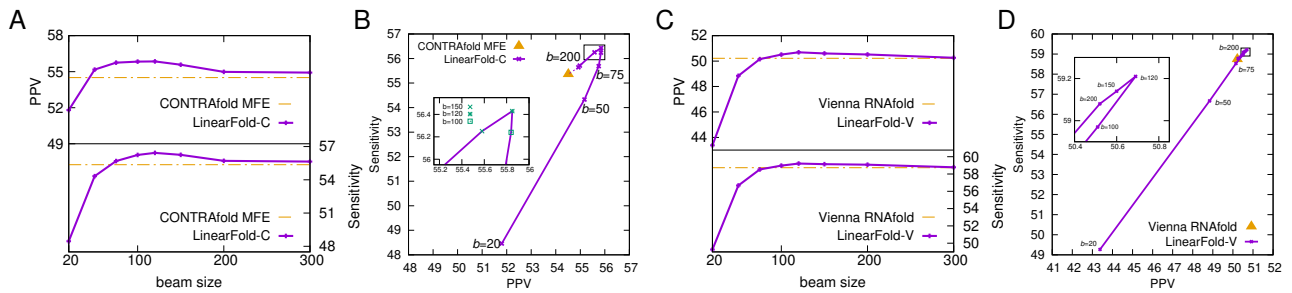


Fig. 6. Impacts of beam size on prediction accuracy. **A and C:** PPV and Sensitivity with varying beam size for LinearFold-C (**A**) and LinearFold-V (**C**); **B and D:** PPV-sensitivity tradeoff for LinearFold-C (**B**) and LinearFold-V (**D**). Note that LinearFold with $b = \infty$ is exact search in $O(n^3)$ time (Idea 2) and produces identical results to the baselines.

shown in Fig. 4C. Combined with Supplementary Fig. S11, we conclude that LinearFold is more selective in predicting long-range base pairs (higher PPV), but nevertheless predicts *more* such pairs that are correct (higher Sensitivity). Supplementary Fig. S12B–C further shows that both LinearFold-C and LinearFold-V correct the severe overprediction of those long-range base pairs in exact search baselines.

Interestingly, even though our algorithm scans 5'-to-3', the accuracy does not degrade toward the 3'-end, shown in Supplementary Fig. S14.

3.3 Search Quality

Above we used beam size 100. Now we investigate the impacts of varying beam size. We first study its impact on search quality. Since our search is approximate, we quantify the notion of *search error* (Huang and Sagae, 2010) as the difference in score or free energy between \hat{y} , the optimal structure returned by exact search, and \bar{y} , the one found by our linear-time beam search, i.e.,

$$sc_w(\mathbf{x}, \hat{y}) - sc_w(\mathbf{x}, \bar{y}).$$

The smaller this gap, the better the search quality. Figure 5A shows that search error shrinks with beam size, quickly converging to 0 (exact search); Figure 5B–C show that the search error (at $b = 100$) grows linearly with sequence length, indicating that our search quality does not degrade with longer sequences (the average search error per nucleotide stays the same).

3.4 Impacts of Beam Size on Prediction Accuracy

Figure 6A plots PPV and sensitivity as a function of beam size. LinearFold-C outperforms CONTRAFold MFE in both PPV and sensitivity with $b \geq 75$ and is stable with $b \in [100, 150]$. Figure 6B shows the tradeoff between PPV and sensitivity. Both PPV and sensitivity increase initially with beam size, culminating at $b=120$, and then decrease, converging to exact search. We do not tune the beam size on any dataset and use the round number of 100 as default. Figures 6C–D show a similar trend for LinearFold-V.

3.5 Example Predictions: Group I Intron, 16S & 23S rRNAs

Fig. 7 visualizes the predicted secondary structures from three RNA families: *Cryptothallus mirabilis* Group I Intron, *Bacillus subtilis* 16S rRNA, and *Escherichia coli* 23S rRNA. We observe that LinearFold substantially reduces false positives (shown in red), especially on the CONTRAFold model. It also correctly predicts many (clusters of) long-range base pairs (true positives, shown in blue), e.g., in *C. mirabilis* Group I Intron with LinearFold-C (Fig. 7D, pair distance 237nt), *B. subtilis* 16S rRNA with LinearFold-C (Fig. 7E, pair distance 460nt), *E. coli* 23S rRNA with both LinearFold-C and LinearFold-V (Figs. 7F and 7L, pair distance 582nt). This reconfirms LinearFold's advantage in predicting long-range base pairs shown in Fig. 4C. Moreover, LinearFold is able to predict the longest 5'-3' pairs, as shown in *E. coli* 23S rRNA with LinearFold-V (Fig. 7L, pair distance 2,901nt). In most cases (except LinearFold-V on *B. subtilis* 16S rRNA, Fig. 7K), LinearFold improves substantially over the corresponding baselines. By contrast, local folding

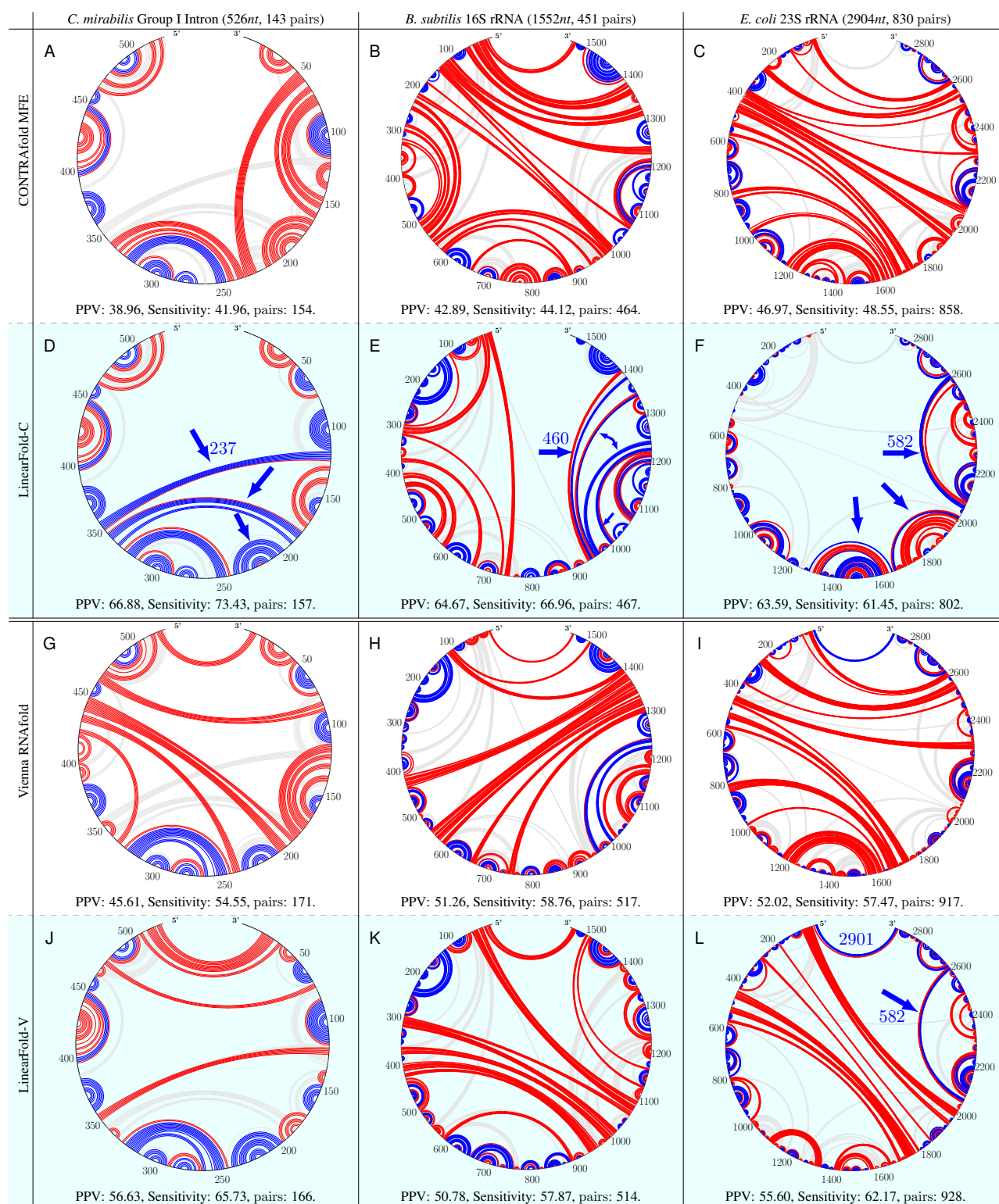


Fig. 7. Circular plots of the prediction results on three RNA sequences (from three different RNA families) comparing the baselines (A–C: CONTRAFold MFE; G–I: Vienna RNAfold) and our LinearFold (D–F: LinearFold-C; J–L: LinearFold-V). Correctly predicted base pairs are in blue (true positives), incorrectly predicted pairs in red (false positives), and missing true base pairs in light gray (false negatives). Each plot is clockwise from 5' to 3'. We can observe that (1) our LinearFold greatly reduces the false positives, esp. on CONTRAFold; (2) our LinearFold correctly predicts many long-range pairs, e.g., LinearFold-C on all three sequences (D–F) and LinearFold-V on *E. coli* 23S rRNA (L); (3) our LinearFold is able to predict the longest 5'-3' pairs, even with the beam size of 100, which is an order of magnitude smaller than the sequence lengths of 16S and 23S rRNAs. (4) in almost all cases (except for LinearFold-V on *B. subtilis* 16S rRNA (K)), LinearFold substantially outperforms the corresponding baseline.

methods do not predict any long-range pairs, shown in Fig. 8. We use `rnafold --maxBPspan 150` for local folding, and this limit of 150 is the largest default limit in the local folding literature and softwares.

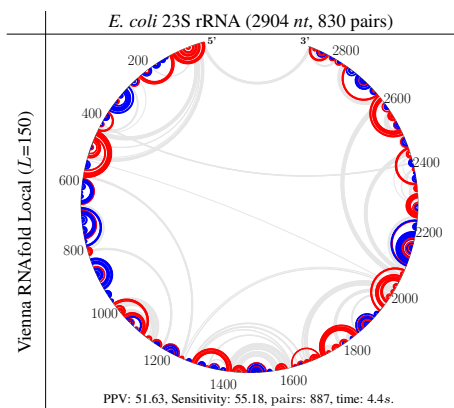


Fig. 8. Circular plots of prediction results using the local folding mode of Vienna RNAfold (which only predicts local pairs no more than 150 nt apart) on the *E. coli* 23S rRNA (corresponding to Figure 7D). Moreover, the $O(nL^2)$ -time local folding (with default $L = 150$) is twice as slow as the $O(nb \log b)$ -time LinearFold-V (with default $b = 100$).

4 Discussion

There are several reasons why our beam search algorithm, though approximate, outperforms the exact search baselines in terms of accuracy (esp. in 16S and 23S rRNAs and long-range base pairs).

1. First, the scoring functions are imperfect, so it is totally possible for a suboptimal structure (in terms of model score or free energy) to be more accurate than the optimal-score structure. For example, it was well studied that while the lowest free energy structure contains only 72.9% of the actual base pairs (given a dataset), a structure containing 86.1% of them can be found with a free energy within 4.8% of the optimal structure (Zuker et al., 1991; Mathews et al., 1999).
2. Secondly, the beam search algorithm prunes lower-scoring (sub)structures at each step, requiring the surviving (sub)structures and the final result to be highly scored for each prefix. Our results suggest that this extra constraint, like “regularization”, could compensate for the inaccuracy of the (physical or machine-learning) model, as LinearFold *systematically* picks a more accurate suboptimal structure without knowing the ground truth; indeed, this seemingly surprising phenomenon has been observed before in computational linguistics (Huang and Sagae, 2010) which inspired this work.
3. Finally, our LinearFold algorithm resembles cotranscriptional folding where RNA molecules start to fold immediately before being fully transcribed (Gultyaev et al., 1995; Meyer and Miklos, 2004). This is analogous to psycholinguistic evidence that humans incrementally parse a sentence before it is fully read or heard (Frazier and Rayner, 1982). We hypothesize that some RNA sequences have evolved to fold co-transcriptionally (Meyer and Miklos, 2004), thus making our 5’-to-3’ incremental approach more accurate than bottom-up baselines. Supplementary Fig. S15B shows a slight preference for 5’-to-3’ order over 3’-to-5’.

There are other algorithmic efforts to speed up RNA folding, including an $O(n^3/\log n)$ algorithm using the Four-Russians method (Venkatachalam et al., 2014), and two other sub-cubic algorithms inspired by fast matrix multiplication and context-free parsing (Zakov et al., 2011; Bringmann et al., 2016). We note that all of them are based on the classical cubic-time bottom-up algorithm, and thus orthogonal to our left-to-right approach. There also exists a linear-time algorithm (Rastegari and Condon, 2005) to analyze a *given* structure, but not to predict one *de novo*.

5 Conclusion and Future Work

We designed an $O(n)$ -time, $O(n)$ -space, approximate search algorithm, using incremental dynamic programming plus beam search, and apply this algorithm to both machine-learned and thermodynamic models. Besides the linearity in both time and memory (Fig. 3), we also found:

1. Though LinearFold uses only a fraction of time and memory compared to existing algorithms, our predicted structures are even more accurate overall in both PPV and sensitivity and on both machine-learned and thermodynamic models (see Fig. 4).
2. The accuracy improvement of LinearFold is more pronounced on longer families such as 16S and 23S rRNAs (see Figs. 4 and 7).
3. LinearFold is also more accurate than the baselines at predicting long-range base pairs over 500nt apart (Figs. 4C), which is well known to be challenging for the current models (Amman et al., 2013).
4. Although the performance of LinearFold depends on the beam size b , the number of base pairs and the accuracy of prediction are stable when b is in the range of 100–200.

There is a crucial difference between our LinearFold and local folding algorithms (Kiryu et al., 2008; Bernhart et al., 2006; Lange et al., 2012) that can only predict pairs up to a certain distance. Theoretical and empirical studies found several evidences that *unboundedly* long-distance pairs are actually quite common in natural RNA structures: (a) the length of the longest base pair grows nearly linearly with sequence length n (Li and Reidys, 2018); (b) the physical distance between the 5’–3’ ends in folded structures is short and nearly constant (Lai et al., 2018; Yoffe et al., 2011; Leija-Martínez et al., 2014).

Our work has several potential extensions.

1. It is possible that LinearFold can be extended to calculate the partition function and base pair probabilities for natural RNA sequences with well-defined structures, since the classical method for that task, the McCaskill (1990) algorithm, is isomorphic in structure to the cubic-time algorithms that are used as baselines in this paper.
2. This linear-time approach to calculate base pair probabilities should facilitate the linear-time identification of pseudoknots, by either replacing the cubic-time McCaskill algorithm with a linear-time one in those heuristic pseudoknot-prediction programs (Bellaousov and Mathews, 2010; Sato et al., 2011), or linearizing a supercubic-time dynamic program for direct prediction with pseudoknots (Dirks and Pierce, 2003; Reeder and Giegerich, 2004).
3. We will test the hypothesis that our beams potentially capture cotranscriptional folding with empirical data on cotranscriptional folding (Watters et al., 2016).
4. Being linear-time, LinearFold also facilitates faster parameter training than the cubic-time CONTRAfold using structured prediction methods (Huang et al., 2012), and we envision a more accurate LinearFold using a model tailored to its own search.

Acknowledgements

We would like to thank the reviewers for suggestions, Rhiju Das for encouragement and early adoption of LinearFold into the EteRNA game, James Cross for help in algorithm design, and Juneki Hong and Liang Zhang for proofreading.

Author Contributions

L.H. conceived the idea and directed the project. L.H., D.D., and K.Z. designed algorithms. L.H. and D.D. wrote a Python prototype, and K.Z., D.D., and H.Z. wrote the fast C++ version. D.H.M. and D.H. guided the evaluation that H.Z. and D.D. carried out. L.H., D.D., and H.Z. wrote the manuscript; D.H.M. and D.H. revised it. K.L. made the webserver.

Funding

This project was supported in part by National Science Foundation [IIS-1656051 and IIS-1817231 to L.H.], National Institutes of Health [R56 AG053460 and R21 AG052950 to D.H., and R01 GM076485 to D.H.M.].

References

Aghaepour, N. and Hoos, H. H. (2013). Ensemble-based prediction of RNA secondary structures. *BMC bioinformatics*, **14**(139), 1.

Amman, F., Bernhart, S. H., Doose, G., Hofacker, I. L., Qin, J., Stadler, P. F., and Will, S. (2013). The trouble with long-range base pairs in RNA folding. In J. Setubal and N. Almeida, editors, *Proceedings of the 8th Brazilian Symposium on Bioinformatics*, pages 1–11, Recife, Brazil. Springer International Publishing Switzerland.

Andronescu, M., Condon, A., Hoos, H. H., Mathews, D. H., and Murphy, K. P. (2007). Efficient parameter estimation for RNA secondary structure prediction. *Bioinformatics*, **23**(13), i19–i28.

Angelbello, A. J., Chen, J. L., Childs-Disney, J. L., Zhang, P., Wang, Z.-F., and Disney, M. D. (2018). Using genome sequence to enable the design of medicines and chemical probes. *Chemical reviews*, **118**(4), 1599–1663.

Bellaousov, S. and Mathews, D. H. (2010). Probknot: fast prediction of RNA secondary structure including pseudoknots. *RNA*, **16**(10), 1870–1880.

Bernhart, S. H., Hofacker, I. L., and Stadler, P. F. (2006). Local RNA base pairing probabilities in large sequences. *Bioinformatics*, **22**(5), 614–615.

Bringmann, K., Grandoni, F., Saha, B., and Williams, V. V. (2016). Truly sub-cubic algorithms for language edit distance and RNA-folding via fast bounded-difference min-plus product. In *2016 IEEE 57th Annual Symposium on Foundations of Computer Science (FOCS)*, pages 375–384, New Brunswick, NJ, USA. IEEE.

Castanotto, D. and Rossi, J. J. (2009). The promises and pitfalls of RNA-interference-based therapeutics. *Nature*, **457**(7228), 426–433.

Childs-Disney, J. L., Wu, M., Puschchnikov, A., Aminova, O., and Disney, M. D. (2007). A small molecule microarray platform to select RNA internal loop-ligand interactions. *ACS Chemical Biology*, **2**(11), 745–754.

Crooke, S. (2004). Antisense strategies. *Current Molecular Medicine*, **4**(5), 465–487.

Dirks, R. M. and Pierce, N. A. (2003). A partition function algorithm for nucleic acid secondary structure including pseudoknots. *Journal of computational chemistry*, **24**(13), 1664–1677.

Do, C., Woods, D., and Batzoglou, S. (2006). Contrafold: RNA secondary structure prediction without physics-based models. *Bioinformatics*, **22**(14), e90–e98.

Eddy, S. R. (2001). Non-coding RNA genes and the modern RNA world. *Nature Reviews Genetics*, **2**(12), 919–929.

Frazier, L. and Rayner, K. (1982). Making and correcting errors during sentence comprehension: Eye movements in the analysis of structurally ambiguous sentences. *Cognitive psychology*, **14**(2), 178–210.

Fu, Y., Xu, Z. Z., Lu, Z. J., Zhao, S., and Mathews, D. H. (2015). Discovery of novel ncRNA sequences in multiple genome alignments on the basis of conserved and stable secondary structures. *PLoS One*, **10**(6), e0130200.

Gareiss, P. C., Sobczak, K., McNaughton, B. R., Palde, P. B., Thornton, C. A., and Miller, B. L. (2008). Dynamic combinatorial selection of molecules capable of inhibiting the (CUG) repeat RNA-MBNL1 interaction in vitro: discovery of lead compounds targeting myotonic dystrophy (DM1). *Journal of the American Chemical Society*, **130**(48), 16254–16261.

Gilbert, W. (1986). Origin of life: The RNA world. *Nature*, **319**(6055).

Gruber, A., Findeliss, S., Washietl, S., Hofacker, I., and Stadler, P. F. (2010). RNAz 2.0: improved noncoding RNA detection. In *Pacific Symposium on Biocomputing*, volume 15, pages 69–79. World Scientific Publishing.

Gulyaev, A. P., Van Batenburg, F., and Pleij, C. W. (1995). The computer simulation of RNA folding pathways using a genetic algorithm. *Journal of molecular biology*, **250**(1), 37–51.

Hofacker, I. L. and Lorenz, R. (2014). *Predicting RNA structure: advances and limitations*. Humana Press, Totowa, NJ, USA.

Huang, L. and Chiang, D. (2005). Better k -best Parsing. In *Proceedings of the Ninth International Workshop on Parsing Technologies (IWPT-2005)*, pages 53–64. ACL.

Huang, L. and Sagae, K. (2010). Dynamic programming for linear-time incremental parsing. In *Proceedings of ACL 2010*, page 1077aL⁺1086, Uppsala, Sweden. ACL.

Huang, L., Fayong, S., and Guo, Y. (2012). Structured perceptron with inexact search. In *Proceedings of NAACL 2012*, pages 142–151. ACL.

Joyce, G. F. (1994). In vitro evolution of nucleic acids. *Current opinion in structural biology*, **4**(3), 331–336.

Kasami, T. (1965). An efficient recognition and syntax analysis algorithm for context-free languages. Technical Report AFCRL-65-758, AFCRL.

Kiryu, H., Kin, T., and Asai, K. (2008). Rfold: an exact algorithm for computing local base pairing probabilities. *Bioinformatics*, **24**(3), 367–373.

Knuth, D. (1965). On the translation of languages from left to right. *Information and Control*, **8**, 607–639.

Lai, W.-J. C., Kayedkhordeh, M., Cornell, E. V., Farah, E., Bellaousov, S., Rietmeijer, R., Mathews, D. H., and Ermolenko, D. N. (2018). The formation of intramolecular secondary structure brings mRNA ends in close proximity. *Nature Communications*, **9**(1), 4328.

Lange, S. J., Maticzka, D., Möhl, M., Gagnon, J. N., Brown, C. M., and Backofen, R. (2012). Global or local? predicting secondary structure and accessibility in mRNAs. *Nucleic Acids Research*, **40**(12), 5215–5226.

Leija-Martínez, N., Casas-Flores, S., Cadena-Nava, R. D., Roca, J. A., Mendez-Cabañas, J. A., Gomez, E., and Ruiz-García, J. (2014). The separation between the 5'-3' ends in long RNA molecules is short and nearly constant. *Nucleic Acids Research*, **42**(22), 13963–13968.

Li, T. J. and Reidys, C. M. (2018). The rainbow spectrum of RNA secondary structures. *Bulletin of mathematical biology*, **80**(6), 1514–1538.

Licon, A., Taufer, M., Leung, M.-Y., and Johnson, K. L. (2010). A dynamic programming algorithm for finding the optimal segmentation of an RNA sequence in secondary structure predictions. In *2nd International Conference on Bioinformatics and Computational Biology*, pages 165–170. ACM.

Lorenz, R., Bernhart, S. H., Zu Siederdisen, C. H., Tafer, H., Flamm, C., Stadler, P. F., and Hofacker, I. L. (2011). ViennaRNA package 2.0. *Algorithms for Molecular Biology*, **6**(1), 1.

Lu, Z. J. and Mathews, D. H. (2008). Efficient siRNA selection using hybridization thermodynamics. *Nucleic Acids Research*, **36**(2), 640–647.

Mathews, D. H. and Turner, D. H. (2006). Prediction of RNA secondary structure by free energy minimization. *Current Opinion in Structural Biology*, **16**(3), 270–278.

Mathews, D. H., Sabina, J., Zuker, M., and Turner, D. H. (1999). Expanded sequence dependence of thermodynamic parameters improves prediction of RNA secondary structure. *Journal of molecular biology*, **288**(5), 911–940.

Mathews, D. H., Disney, M. D., Childs, J. L., Schroeder, S. J., Zuker, M., and Turner, D. H. (2004). Incorporating chemical modification constraints into a dynamic programming algorithm for prediction of RNA secondary structure. *Proceedings of the National Academy of Sciences of the United States of America*, **101**(19), 7287–7292.

McCaskill, J. S. (1990). The equilibrium partition function and base pair binding probabilities for RNA secondary structure. *Biopolymers*, **29**(6-7), 1105–1119.

Meyer, I. M. and Miklos, I. (2004). Co-transcriptional folding is encoded within RNA genes. *BMC molecular biology*, **5**(1), 10.

Nussinov, R., Pieczenik, G., Griggs, J. R., and Kleitman, D. J. (1978). Algorithms for loop matchings. *SIAM Journal on Applied mathematics*, **35**(1), 68–82.

Palde, P. B., Ofori, L. O., Gareiss, P. C., Lerea, J., and Miller, B. L. (2010). Strategies for recognition of stem-loop RNA structures by synthetic ligands: Application to the HIV-1 frameshift stimulatory sequence. *Journal of Medicinal Chemistry*, **53**(16), 6018–6027.

Rastegari, B. and Condon, A. (2005). Linear time algorithm for parsing RNA secondary structure. In *International Workshop on Algorithms in Bioinformatics*, pages 341–352. Springer.

Reeder, J. and Giegerich, R. (2004). Design, implementation and evaluation of a practical pseudoknot folding algorithm based on thermodynamics. *BMC bioinformatics*, **5**(1), 1.

Sato, K., Hamada, M., Asai, K., and Mituyama, T. (2009). Centroidfold: a web server for RNA secondary structure prediction. *Nucleic Acids Research*, **37**(suppl_2), W277–W280.

Sato, K., Kato, Y., Hamada, M., Akutsu, T., and Asai, K. (2011). Ipknnot: fast and accurate prediction of RNA secondary structures with pseudoknots using integer programming. *Bioinformatics*, **27**(13), i85–i93.

Sazani, P., Gemignani, F., Kang, S.-H., Maier, M., Manoharan, M., Persmark, M., Bortner, D., and Kole, R. (2002). Systemically delivered antisense oligomers

- upregulate gene expression in mouse tissues. *Nature biotechnology*, **20**(12), 1228–1233.
- Seetin, M. G. and Mathews, D. H. (2012). *RNA structure prediction: an overview of methods*. Humana Press, Totowa, NJ, USA.
- Sloma, M. and Mathews, D. (2016). Exact calculation of loop formation probability identifies folding motifs in RNA secondary structures. *RNA*, **22**, 1808–1818.
- Stephens, Z. D., Lee, S. Y., Faghri, F., Campbell, R. H., Zhai, C., Efron, M. J., Iyer, R., Schatz, M. C., Sinha, S., and Robinson, G. E. (2015). Big data: astronomical or genetical? *PLoS Biology*, **13**(7), e1002195.
- Tafer, H., Ameres, S. L., Obernosterer, G., Gebeshuber, C. A., Schroeder, R., Martinez, J., and Hofacker, I. L. (2008). The impact of target site accessibility on the design of effective siRNAs. *Nature biotechnology*, **26**(5), 578–583.
- The RNAcentral Consortium (2017). RNAcentral: a comprehensive database of non-coding RNA sequences. *Nucleic Acids Research*, **45**(D1), D128–D134.
- Tomita, M. (1988). Graph-structured stack and natural language parsing. In *Proceedings of ACL*, page 249–257. ACL.
- Venkatachalam, B., Gusfield, D., and Frid, Y. (2014). Faster algorithms for RNA-folding using four-russians method. *Algorithms for Molecular Biology*, **9**(1), 5.
- Washietl, S., Will, S., Hendrix, D. A., Goff, L. A., Rinn, J. L., Berger, B., and Kellis, M. (2012). Computational analysis of noncoding RNAs. *Wiley Interdisciplinary Reviews: RNA*, **3**(6), 759–778.
- Watters, K. E., Strobel, E. J., Angela, M. Y., Lis, J. T., and Lucks, J. B. (2016). Cotranscriptional folding of a riboswitch at nucleotide resolution. *Nature structural & molecular biology*, **23**(12), 1124.
- Watts, J. M., Dang, K. K., Gorelick, R. J., Leonard, C. W., Bess Jr, J. W., Swanstrom, R., Burch, C. L., and Weeks, K. M. (2009). Architecture and secondary structure of an entire HIV-1 RNA genome. *Nature*, **460**(7256), 711–716.
- Yoffe, A. M., Prinsen, P., Gelbart, W., and Ben-Shaul, A. (2011). The ends of a large RNA molecule are necessarily close. *Nucleic Acids Research*, **39**(1), 292–299.
- Younger, D. H. (1967). Recognition and parsing of context-free languages in time n^3 . *Information and Control*, **10**, 189–208.
- Zakov, S., Tsur, D., and Ziv-Ukelson, M. (2011). Reducing the worst case running times of a family of RNA and CFG problems, using valiant's approach. *Algorithms for Molecular Biology*, **6**(1), 20.
- Zhao, Y., Li, H., Fang, S., Kang, Y., Hao, Y., Li, Z., Bu, D., Sun, N., Zhang, M. Q., Chen, R., et al. (2016). Noncode 2016: an informative and valuable data source of long non-coding RNAs. *Nucleic Acids Research*, **44**(D1), D203–D208.
- Zuker, M. and Stiegler, P. (1981). Optimal computer folding of large RNA sequences using thermodynamics and auxiliary information. *Nucleic Acids Research*, **9**(1), 133–148.
- Zuker, M., Jaeger, J. A., and Turner, D. H. (1991). A comparison of optimal and suboptimal RNA secondary structures predicted by free energy minimization with structures determined by phylogenetic comparison. *Nucleic Acids Research*, **19**(10), 2707–2714.

Supporting Information

LinearFold: Linear-Time Approximate RNA Folding by 5'-to-3' Dynamic Programming and Beam Search

Liang Huang, He Zhang, Dezhong Deng, Kai Zhao, Kaibo Liu, David Hendrix, and David H. Mathews

A Extra Definitions

In Section 2.1, we sketched the definition of the set of allowed pseudoknot-free secondary structures

$$\mathcal{Y}(\mathbf{x}) = \{\mathbf{y} \in \{., (,)\}^{|\mathbf{x}|} \mid \text{balanced}(\mathbf{y}), \text{valid}(\mathbf{x}, \text{pairs}(\mathbf{y}))\}$$

Here we complete it. First we denote $\text{depth}(\mathbf{y}) = \sum_i (\mathbb{1}[y_i = (] - \mathbb{1}[y_i =)])$ to be the difference in counts between “(” and “)” in \mathbf{y} , and then $\text{balanced}(\mathbf{y})$ is true iff.:

$$\forall i, \text{depth}(y_1 \dots y_i) \geq 0; \text{ and } \text{depth}(\mathbf{y}) = 0.$$

We next define the set of pairs in \mathbf{y} :

$$\text{pairs}(\mathbf{y}) = \{(i, j) \mid y_i = (, y_j =), \text{balanced}(y_i \dots y_j)\}$$

and $\text{valid}(\mathbf{x}, S)$ checks if all pairs in set S are valid for \mathbf{x} , i.e., it returns true iff.:

$$\forall (i, j) \in S, x_i x_j \in \{\text{CG, GC, AU, UA, GU, UG}\}$$

We also define $\text{unpaired}(\mathbf{y}) = \{i \mid y_i = .\}$ to be set of unpaired indices in \mathbf{y} .

B Actual Scoring Functions

The actual scoring functions used by CONTRAfold, RNAfold, and our LinearFold decompose into individual loops:

$$\begin{aligned} sc_{\mathbf{w}}(\mathbf{x}, \mathbf{y}) = & \sum_{(i,j) \in \text{hairpin_loops}(\mathbf{y})} sc_{\mathbf{w}}^{\text{H}}(\mathbf{x}, i, j) + \sum_{(i,j,k,l) \in \text{single_loops}(\mathbf{y})} sc_{\mathbf{w}}^{\text{S}}(\mathbf{x}, i, j, k, l) \\ & + \sum_{m \in \text{multi_loops}(\mathbf{y})} sc_{\mathbf{w}}^{\text{M}}(\mathbf{x}, m) + \sum_{(i,j) \in \text{external_loops}(\mathbf{y})} sc_{\mathbf{w}}^{\text{E}}(\mathbf{x}, i, j). \end{aligned} \quad (3)$$

where $sc_{\mathbf{w}}^{\text{H}}(\mathbf{x}, \cdot, \cdot)$, $sc_{\mathbf{w}}^{\text{S}}(\mathbf{x}, \cdot, \cdot, \cdot, \cdot)$, $sc_{\mathbf{w}}^{\text{M}}(\mathbf{x}, \cdot)$, $sc_{\mathbf{w}}^{\text{E}}(\mathbf{x}, \cdot, \cdot)$ are scores of hairpin loop, single loop (including bulge and internal loop and stacking), multiloop and external loop, respectively. Multiloop score can be further decomposed into each adjacent base pair $(i, j) \in m$:

$$sc_{\mathbf{w}}^{\text{M}}(\mathbf{x}, m) = w_{\text{base}}^{\text{multi}} + w_{\text{unpair}}^{\text{multi}} \cdot |\text{unpaired}(m)| + \sum_{(i,j) \in m} w_{\text{bp}}^{\text{multi}}(\mathbf{x}, i, j) \quad (4)$$

For example, if $\mathbf{y} = . (. (. . .) (. . .)) .$, then $\text{multi_loops}(\mathbf{y})$ is a singleton-set containing $m = ((2, 16), (4, 8), (9, 15))$ with $\text{unpaired}(m) = \{3\}$, $\text{hairpin_loops}(\mathbf{y}) = \{(4, 8), (10, 14)\}$, $\text{single_loops}(\mathbf{y}) = \{(9, 10, 14, 15)\}$, and $\text{external_loops}(\mathbf{y}) = \{(0, 2), (16, 17)\}$.

The thermodynamic model in Vienna RNAfold scores each type of loop using several feature templates such as hairpin/bulge/internal loop lengths, terminal mismatches, helix stacking, helix closing, etc. The machine-learned model in CONTRAfold replaces energies in the above framework with model weights learned from data. Figure S16 implement LinearFold for this scoring function.

C Extra Results Tables and Figures

Tables S11 & S12 detail the accuracy results (PPV & Sensitivity) from Figure 4. We choose the ArchiveII dataset (Sloma and Mathews, 2016), a diverse set of over 3,000 RNA sequences with known secondary structures. But since the current CONTRAfold machine-learned model (v2.02) is trained on the S-Processed dataset (Andronescu *et al.*, 2007) we removed those sequences that appeared in the S-Processed dataset. The resulting dataset we used contains 2,889 sequences over 9 families, with an average length of 222.2 *nt*.

We sample RNACentral dataset by evenly splitting the length range from 1, 000 to 244, 296 (the longest sequence) into 30 bins by log-scale, and for each bin randomly select one sequence.

Due to the uncertainty of base-pair matches existing in comparative analysis and the fact that there is fluctuation in base pairing at equilibrium, we consider a base pair to be correctly predicted if it is also displaced by one nucleotide on a strand (Sloma and Mathews, 2016). Generally, if a pair (i, j) is in the predicted structure, we consider it a correct prediction if one of (i, j) , $(i - 1, j)$, $(i + 1, j)$, $(i, j - 1)$, $(i, j + 1)$ is in the ground truth structure. We also report the accuracy using exact base pair matching instead of this method, in Table S12. Both sensitivity and PPV are reported. Generally, if $\hat{\mathbf{y}}$ is the predicted structure and \mathbf{y}^* is the ground truth, we have $\text{Sensitivity} = \frac{|\text{pairs}(\hat{\mathbf{y}}) \cap \text{pairs}(\mathbf{y}^*)|}{|\text{pairs}(\hat{\mathbf{y}})|}$, and $\text{PPV} = \frac{|\text{pairs}(\hat{\mathbf{y}}) \cap \text{pairs}(\mathbf{y}^*)|}{|\text{pairs}(\mathbf{y}^*)|}$.

The following Figure details the impact of beam size on the number of pairs predicted. Figure S12A plots the number of pairs predicted (per nucleotide) with varying beam size, compared with ground truth (both with and without the pseudoknotted pairs). It shows that (a) there are on average

Family	# of seqs		avg. length	CONTRAFold [*]		LinearFold-C [*]		CONTRAFold		LinearFold-C		Vienna RNAfold		LinearFold-V	
	total	used		PPV	sens	Δ PPV	Δ sens	PPV	sens	Δ PPV	Δ sens	PPV	sens	Δ PPV	Δ sens
tRNA	557	74	77.3	68.89	70.54	+0.00	+0.00	69.05	70.54	+0.00	+0.00	63.51	72.92	+0.24	+0.19
5S rRNA	1,283	1,125	118.8	73.66	73.74	+0.00	+0.00	75.52	75.61	+0.00	+0.00	59.55	65.96	+0.03	+0.04
SRP	928	886	186.1	62.73	62.41	-0.07	-0.07	63.27	62.84	-0.04	-0.04	59.91	65.42	[†] +0.35	+0.27
RNaseP	454	182	344.1	48.91	47.90	-0.22	[†] -0.54	48.96	47.67	-0.11	-0.14	47.28	55.15	+0.12	-0.07
tmRNA	462	462	366	44.88	38.61	[†] -0.74	[‡] -0.93	45.74	39.05	[†] -0.67	[‡] -0.82	41.47	46.86	[‡] -0.95	[‡] -1.02
Group I Intron	98	96	424.9	52.62	50.93	+0.84	[†] +0.80	52.36	50.64	+0.87	+0.80	46.81	57.68	[‡] +0.86	[†] +1.02
telomerase RNA	37	37	444.6	45.39	59.19	-0.05	-0.11	45.62	59.30	-0.05	-0.11	41.47	58.20	+0.05	-0.05
16S rRNA	22	22	1,547.90	41.08	41.77	[†] +3.56	[†] +3.09	40.20	41.21	[†] +3.76	[†] +3.26	37.23	44.13	[†] +1.51	+1.59
23S rRNA	5	5	2,927.40	52.47	53.18	[†] +8.65	[†] +5.66	48.05	49.61	[†] +14.03	[†] +9.86	54.79	62.32	+0.33	+0.16
Overall	3,846	2,889	222.2	54.51	55.36	+1.33	+0.88	54.31	55.16	+1.98	+1.42	50.22	58.74	+0.28	+0.24

Table S11. Detailed prediction accuracies in percent, allowing one nucleotide in a pair to be displaced by one position, on the ArchiveII dataset using CONTRAFold MFE, LinearFold-C, Vienna RNAfold and LinearFold-V. This slipping method (Sloma and Mathews, 2016) considers a base pair to be correct if it is slipped by one nucleotide on a strand. ^{*} denotes using sharpturn enabled mode (default in CONTRAFold). Statistical significance are marked by [†]($0.01 \leq p < 0.05$) and [‡]($p < 0.01$). Overall, LinearFold-C outperforms CONTRAFold MFE by +1.33/+0.88 in PPV/sensitivity with sharpturn and by +1.98/+1.42 in PPV/sensitivity without sharpturn, and LinearFold-V outperforms Vienna RNAfold by +0.28/+0.24 in PPV/sensitivity. Among the nine families, LinearFold-C is significantly better on three (Group I Intron, 16S and 23S rRNAs), and LinearFold-V is significantly better on three (SRP, Group I Intron, and 16S rRNAs). We also report the accuracies using exact base pair match in the next Table.

Family	# of seqs		avg. length	CONTRAFold [*]		LinearFold-C [*]		CONTRAFold		LinearFold-C		Vienna RNAfold		LinearFold-V	
	total	used		PPV	sens	Δ PPV	Δ sens	PPV	sens	Δ PPV	Δ sens	PPV	sens	Δ PPV	Δ sens
tRNA	557	74	77.3	67.61	69.12	+0.00	+0.00	67.73	69.12	+0.00	+0.00	61.75	70.98	+0.04	-0.07
5S rRNA	1,283	1,125	118.8	70.68	70.70	+0.00	+0.00	72.60	72.59	+0.00	+0.00	57.28	63.35	-0.14	-0.11
SRP	928	886	186.1	59.14	58.61	-0.05	-0.07	59.67	59.02	-0.04	-0.03	56.58	61.55	-0.09	-0.20
RNaseP	454	182	344.1	47.45	46.39	-0.25	[†] -0.55	47.49	46.15	-0.13	-0.15	45.76	53.28	+0.15	+0.04
tmRNA	462	462	366	42.96	36.94	[†] -0.81	[‡] -0.99	43.83	37.38	[†] -0.72	[‡] -0.85	39.75	44.90	[‡] -1.09	[‡] -1.17
Group I Intron	98	96	424.9	51.21	49.56	+0.80	[†] +0.75	51.03	49.35	+0.82	+0.74	45.49	56.06	[‡] +0.81	[†] +0.97
telomerase RNA	37	37	444.6	43.40	56.58	+0.03	+0.00	43.66	56.72	+0.04	+0.00	39.53	55.40	-0.05	-0.19
16S rRNA	22	22	1,547.90	39.84	40.49	[†] +3.47	[†] +2.99	39.01	39.97	[†] +3.62	[†] +3.13	35.65	42.26	[†] +1.33	+1.39
23S rRNA	5	5	2,927.40	50.56	51.24	[†] +8.51	[†] +5.60	46.46	47.97	[†] +13.54	[†] +9.47	53.20	60.50	+0.07	-0.12
Overall	3,846	2,889	222.2	52.54	53.29	+1.30	+0.86	52.39	53.14	+1.90	+1.37	48.33	56.48	+0.11	+0.06

Table S12. The prediction accuracies using exact base-pair matching. Statistical significance are marked by [†]($0.01 \leq p < 0.05$) and [‡]($p < 0.01$). Overall, LinearFold-C outperforms CONTRAFold MFE by +1.30/+0.86 in PPV/sensitivity with sharpturn and by +1.90/+1.37 in PPV/sensitivity without sharpturn, and LinearFold-V outperforms Vienna RNAfold by +0.11 PPV and +0.06 sensitivity. Among the nine families, LinearFold-C is significantly better on three (Group I Intron, 16S and 23S rRNAs), and LinearFold-V is significantly better on two (Group I Intron and 16S rRNAs).

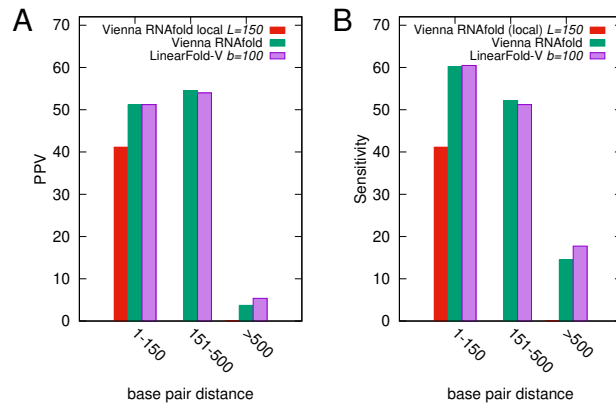


Fig. S11. Comparison of LinearFold-V with Vienna RNAfold and its local folding mode in terms of PPV/Sensitivity of base pairs in certain distance ranges across all sequences. LinearFold-V is more accurate in long-range base pairs (500+nt) in both PPV and Sensitivity. See Fig. 4C for the corresponding results for LinearFold-C.

0.2776 pairs per nucleotide in this dataset (meaning about 55.5% of all nucleotides are paired) and 7.6% pairs are pseudoknotted; (b) ViennaRNA tends to overpredict, while CONTRAFold tends to underpredict; (c) our algorithm predicts more pairs with larger beam size; and (d) with the default beam size, it predicts almost the same amounts of pairs as the baselines (only 0.0002 and 0.0012 pairs less per nucleotide, respectively). This is also confirmed by Fig. S12B–C.

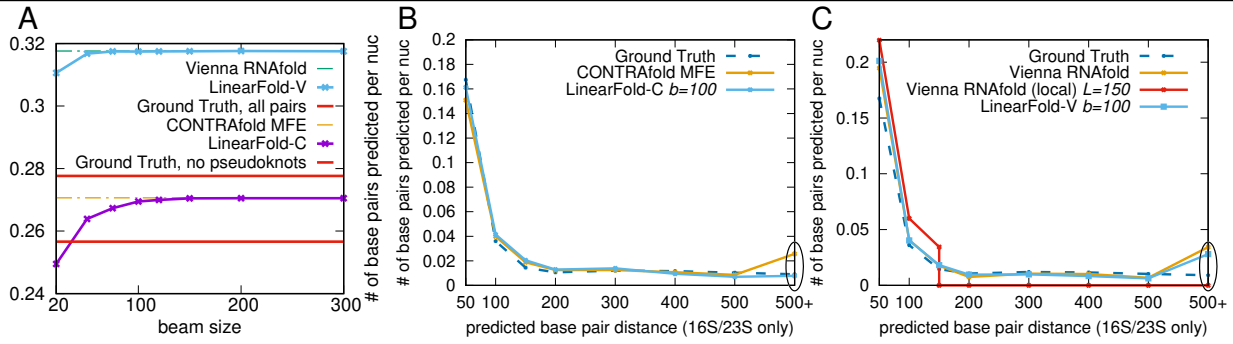


Fig. SI2. A: The number of pairs predicted per nucleotide with varying beam size, comparing these methods and the ground truth (with and without pseudoknots (PK)); B and C: Length distributions of the predicted base pairs using different methods, on the 16S/23S rRNAs in the ArchiveII dataset. Here we plot the number of both predicted and ground truth base pairs (including pseudoknots) in each of the following ranges: (0, 50], (50, 100], ... (400, 500), [500, ∞). This figure shows that LinearFold-C produces almost the same length distributions with the ground truth, while CONTRAfold severely overpredicts base pairs longer than 500nt apart. Both ViennaRNA and LinearFold-V overpredict in that range, but LinearFold-V is less severe. In C, we also reconfirm the limitation of local folding which does not output any long-range pairs.

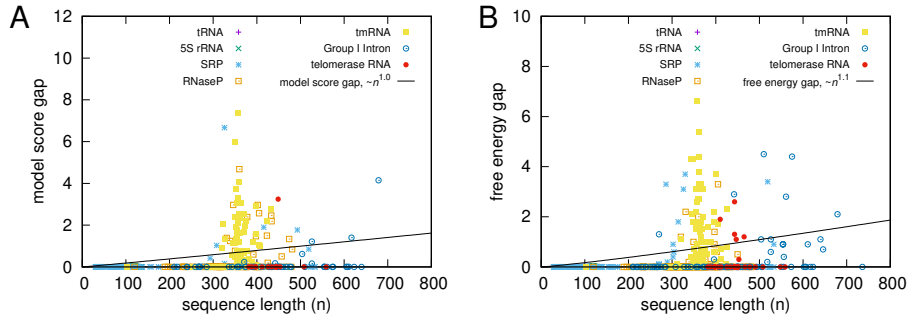


Fig. SI3. Close-ups for Fig. 5 (search error against sequence length) for short sequences. A: LinearFold-C vs. CONTRAfold MFE; B: LinearFold-V vs. Vienna RNAfold. Again, tmRNA is the outlier with disproportionately severe search errors, which can explain the slightly worse accuracies of LinearFold on tmRNA in Fig. 4A. Sequences of 250nt or less have no search errors (i.e., LinearFold with $b=100$ is exact for $n \leq 250$).

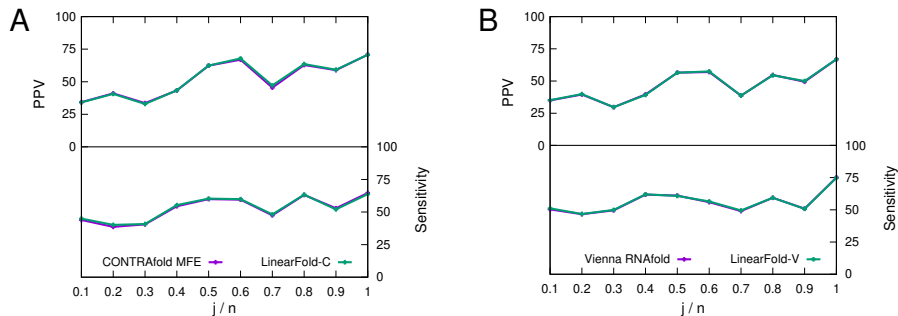


Fig. SI4. PPV/Sensitivity for all pairs (i, j) as a function of j/n where n is the sequence length, i.e., the “proportional distance” of a pair’s right nucleotide to the 5’-end. We bin j/n by $(0, 0.1]$, $(0.1, 0.2]$, ..., $(0.9, 1.0]$. In general, LinearFold performs very similarly to the baselines, and even though it scans 5’-to-3’, the accuracy does not degrade towards the 3’-end.

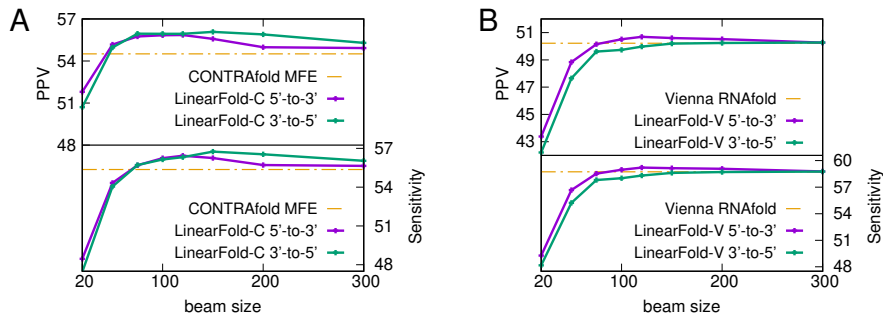


Fig. SI5. Comparing 5’-to-3’ and 3’-to-5’ versions of LinearFold. The physical model (B) seems to prefer the default 5’-to-3’ order.

D Deductive System for the Actual Systems

The following Figure sketches the deductive system for the actual LinearFold system based on the real scoring functions in Section B. For more implementation details, we refer the readers to our released source code at <https://github.com/LinearFold/LinearFold>.

input	$x_1 \dots x_n$	
states	$E \langle 0, j \rangle : \langle \alpha, s \rangle$	prefix structure
	$P \langle i, j \rangle : \langle (\alpha), s \rangle$	pair
	$H \langle i, j \rangle : \langle (\dots), s \rangle$	hairpin candidate
	$M_1 \langle i, j \rangle : \langle (\alpha) \beta, s \rangle$	one or more pairs
	$M_2 \langle i, j \rangle : \langle (\alpha) \beta (\gamma), s \rangle$	two or more pairs
	$M \langle i, j \rangle : \langle (\dots (\alpha) \beta (\gamma) \dots), s \rangle$	multiloop candidate
axiom	$E \langle 0, 1 \rangle : \langle \cdot, 0 \rangle$	goal $E \langle 0, n+1 \rangle : \langle \alpha, _ \rangle$
push	$\frac{E \langle 0, j \rangle : \langle \alpha, s \rangle}{H \langle j, \text{next}(j, j) \rangle : \langle (\dots), 0 \rangle}$	$\text{next}(i, j) \triangleq \min\{k \mid k > j, (x_i, x_k) \text{ match}\}$
Hjump	$\frac{H \langle i, j \rangle : \langle (\dots), s \rangle}{H \langle i, \text{next}(i, j) \rangle : \langle (\dots), s \rangle}$	
skip	$\frac{E \langle 0, j \rangle : \langle \alpha, s \rangle}{E \langle 0, j+1 \rangle : \langle \alpha \cdot, s + sc_{\mathbf{w}}^E(\mathbf{x}, j, j+1) \rangle}$	$\frac{M_1 \langle i, j \rangle : \langle (\alpha) \beta, s \rangle}{M_1 \langle i, j+1 \rangle : \langle (\alpha) \beta \cdot, s + w_{\text{unpair}}^{\text{multi}} \rangle}$
reduce	$\frac{M_1 \langle k, i \rangle : \langle (\alpha) \beta, s' \rangle \quad P \langle i, j \rangle : \langle (\gamma), s \rangle}{M_2 \langle k, j \rangle : \langle (\alpha) \beta (\gamma), s' + s + w_{\text{bp}}^{\text{multi}}(\mathbf{x}, i, j) \rangle}$	
combine	$\frac{E \langle 0, i \rangle : \langle \alpha, s' \rangle \quad P \langle i, j \rangle : \langle (\beta), s \rangle}{E \langle 0, j \rangle : \langle \alpha (\beta), s' + s + sc_{\mathbf{w}}^E(\mathbf{x}, i, j) \rangle}$	
XtoM ₁	$\frac{P \langle i, j \rangle : \langle (\alpha), s \rangle}{M_1 \langle i, j \rangle : \langle (\alpha), s + w_{\text{bp}}^{\text{multi}}(\mathbf{x}, i, j) \rangle}$	$\frac{M_2 \langle i, j \rangle : \langle (\alpha) \beta (\gamma), s \rangle}{M_1 \langle i, j \rangle : \langle (\alpha) \beta (\gamma), s \rangle}$
Mleft	$\frac{M_2 \langle i, j \rangle : \langle (\alpha) \beta (\gamma), s \rangle}{M \langle k, \text{next}(k, j) \rangle : \langle (\dots (\alpha) \beta (\gamma) \dots), s + u \cdot w_{\text{unpair}}^{\text{multi}} \rangle}$	$u = (\text{next}(k, j) - j) + (i - k - 1),$ $i - k - 1 \leq 30$
Mjump	$\frac{M \langle i, j \rangle : \langle (\dots (\alpha) \beta (\gamma) \dots), s \rangle}{M \langle i, \text{next}(i, j) \rangle : \langle (\dots (\alpha) \beta (\gamma) \dots), s + u \cdot w_{\text{unpair}}^{\text{multi}} \rangle}$	$u = \text{next}(i, j) - j$
hairpin	$\frac{H \langle i, j \rangle : \langle (\dots), s \rangle}{P \langle i, j+1 \rangle : \langle (\dots), s + sc_{\mathbf{w}}^H(\mathbf{x}, i, j) \rangle}$	
singleloop	$\frac{P \langle i, j \rangle : \langle (\alpha), s \rangle}{P \langle k, l \rangle : \langle (\dots (\alpha) \dots), s + sc_{\mathbf{w}}^S(\mathbf{x}, i, j, k, l) \rangle}$	$(x_k, x_{l-1}) \text{ match}, (l - j - 1) + (i - k - 1) \leq 30$
multiloop	$\frac{M \langle i, j \rangle : \langle (\dots (\alpha) \beta (\gamma) \dots), s \rangle}{P \langle i, j+1 \rangle : \langle (\dots (\alpha) \beta (\gamma) \dots), s + w_{\text{base}}^{\text{multi}} + w_{\text{bp}}^{\text{multi}}(\mathbf{x}, i, j) \rangle}$	

Fig. SI6. The actual deductive system implemented in LinearFold. Shaded substrings are balanced in brackets. Here $sc_{\mathbf{w}}^E(\mathbf{x}, \cdot, \cdot)$, $w_{\text{base}}^{\text{multi}}$, $w_{\text{bp}}^{\text{multi}}(\mathbf{x}, \cdot, \cdot)$, $w_{\text{unpair}}^{\text{multi}}$, $sc_{\mathbf{w}}^S(\mathbf{x}, \cdot, \cdot, \cdot, \cdot)$, $sc_{\mathbf{w}}^H(\mathbf{x}, \cdot, \cdot)$ are the various energy or scoring parameters (E stands for external loop, multi for multiloop, S for single loop, and H for hairpin loop). The $\text{next}(i, j)$ returns the next position after x_j that can pair with x_i ; this is the “jumping” trick used in CONTRAfold and ViennaRNA. Our final two rules also use this jumping trick in the righthand side loop. The only cubic-time rule is reduce (intermediate step in multiloop), again inspired by CONTRAfold source code.

E Connections between Context-Free Parsing and RNA Folding

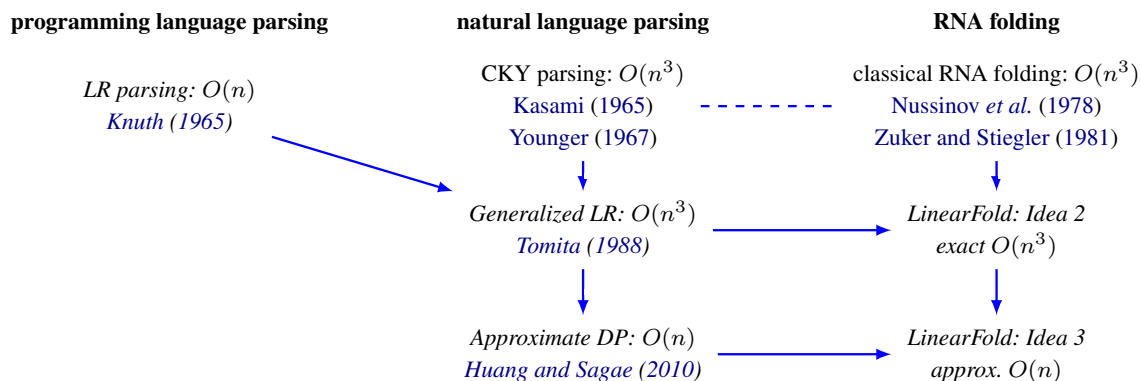


Fig. S17. Our work is inspired by incremental parsing algorithms in both programming language theory and computational linguistics. Left-to-right algorithms are in *italic*; others are bottom-up. The classical bottom-up $O(n^3)$ algorithms are isomorphic between natural language parsing and RNA folding. Knuth's $O(n)$ LR algorithm works only for a small subset of context-free grammars (CFGs), and Tomita generalizes it to arbitrary CFGs, achieving the alternative, left-to-right, $O(n^3)$ algorithm, which inspires LinearFold [Idea 2](#). Our previous work (Huang and Sagae) modernize and generalize Tomita's algorithm, combining it with beam search to achieve linear runtime, which inspires LinearFold [Idea 3](#).